Research Article Vol. 13, No. 6 / 1 Jun 2023 / Optical Materials Express 1579
Optical Materials EXPRESS

Ultra-long-wave infrared broadband absorber based on a nano-resonant ring structure

SHILIN CHEN,[1] ZHIWEI LI,[1,*] LEJIA WU,[1] WENJIE WANG,[2] AND XUDONG TENG[1]

[1]*School of Electronic and Electrical Engineering, Shanghai University of Engineering Science, Shanghai 201620, China*
[2]*Microsystem and Terahertz Research Center, China Academy of Engineering Physics, Chengdu 610200, China*
[*]*zhiwei.li@sues.edu.cn*

Abstract: We designed a four-layer structured absorber (Ti-Si-SiO_2-Ti) in the ultra-long-wave infrared band. The paper applies the bare Ti-SiO_2-Si film to determine the approximate target band of the absorber, and combined with the coupling effect of the top double-ring structure, it greatly enhances the absorber's property, which can make the absorber absorb more than 90% in the range of 14.0-26.3 μm in the ultra-long-wave infrared band. For the complex natural environment in practical applications, the absorber has excellent polarization independence and maintains excellent absorption in the incident environment from 0-60°.

1. Introduction

Unlike natural materials, human-designed and assembled metamaterials have many unique electromagnetic properties and are easily integrated into two-dimensional planar structures for modulating the phase, amplitude, and polarization of electromagnetic waves, which has attracted many researchers to study it intensively. The special properties of metamaterials excited by incident electromagnetic fields have great potential for scientific applications, such as polarization manipulation [1–3], sensors [4–6], energy [7–10], and imaging [11,12]. Among them, metamaterial perfect absorbers (MPA) designed using material properties and their structures have shown excellent results in many fields and become a popular research topic. MPA with only sub wavelength scales usually consist of highly lossy metallic and insulating dielectric materials, and their absorption effects are influenced by the material size and shape.

Nowadays, the widespread use in many hot spots has led to an increasing number of studies on MPA. In essence, MPA is a device that uses the properties of materials and their combined structure to generate high-loss phenomena of electromagnetic waves. In the era of wide application of electromagnetic waves, MPA has great potential for application and is one of the research hotspots in the world. From the recent research results, the absorption effects produced by MPA can be classified into single-peak absorption [13,14], multi-peak absorption [15–17], band absorption [18–21], and tunable band absorption [22–24]. For example, N. I. Landy's group achieved more than 96% peak absorption at 11.6 GHz [25], and L. Zhu et al. Achieved more than 90% uninterrupted absorption in the 300-2000nm band from UV to NIR. Researchers have continued to explore and innovate in absorber structures, and many different absorber structures have emerged, such as multilayer thin film structures consisting of multiple alternating resistive and dielectric layers and a metal layer at the bottom [26], embedded metal-insulator structures with metal ions embedded in an insulating medium [27], metal-insulator-metal (MDM) structures with metal and insulating medium superimposed [28,29], geometric tapering absorbers structures [30,31], etc.

MPAs in the visible to long-wave infrared band are of great value in practical applications. For example, in terms of energy, there are absorbers containing multiple layers of ordinary

#489439 https://doi.org/10.1364/OME.489439
Journal © 2023 Received 7 Mar 2023; revised 21 Apr 2023; accepted 23 Apr 2023; published 8 May 2023

Optical Materials EXPRESS

metal - dielectric planar films, solar absorbers in the wavelength range of 300-2500 nm, the average absorption rate can reach 98.2% [32]. This greatly improves the efficiency of light energy utilization. Infrared wavelengths are widely used in medical and detection imaging fields, and the absorption bandwidth of absorbers is becoming wider. Later, researchers achieved more than 96% absorption in the UV to NIR band from 300-3000 nm, There are also some studies in the field of infrared thermography detection, where absorbers have been designed to achieve absorption in the two main operating bands of infrared devices: mid-wave infrared (MWIR, 3-5 μm) and long-wave infrared (LWIR, 8-14 μm) [33]. In addition, as the commonly used band range for remote sensing is 8-30 μm, which accounts for 80% of the total radiant energy of the earth; by structural design, more than 90% continuous absorption has been achieved in the atmospheric window band of 8-14 μm and the long-wave infrared band of 12-20 μm [34]. Although there are many studies in the infrared band, they are focused on the near-infrared and mid-infrared and less on the ultra-long wave infrared (ULWIR) band (14-30 μm).

In this paper, a metal-dielectric-dielectric-metal (MDDM) periodic structure absorber is simulated, and its average absorption effect can reach more than 96% in the ULWIR band of 14.0-26.3 μm. In the simulation and validation process, the effect of Ti ring number of top layer particles on the absorption effect was first compared. Then, the physical mechanism of the absorption effect was analyzed by electric and magnetic field diagrams, and the structural parameters were verified in detail. Finally, the advantages of the absorber, such as excellent broadband absorption effect, polarization-independence and ultra-wide incidence angle, are demonstrated in various excitation resonance modes.

2. Structure and Performance

In this section, the structure of the MPA and the role of its components in the absorption effect produced in the ultra-long-wave infrared band are analyzed. the structure of the MPA is shown in Fig. 1(a). Structurally, it consists mainly of a periodic structure with a double Ti ring at the top, a composite dielectric layer (lossless dielectric Si and lossy dielectric SiO2) in the middle, and a metallic reflective layer Ti at the bottom. Si has a very small imaginary part of the dielectric constant in the ultra-long wavelength infrared (ULWIR) band, so the absorption dominated by surface plasmon resonance (SPR) can be controlled by adjusting the Si layer The larger imaginary part of the dielectric constant of SiO2 has some intrinsic absorption and is also the main location of the resonance effect in the main cavity layer. After that, the relevant absorption part of the bare Ti-SiO2-Si film is investigated, and it is proved that the target band of the absorber can be roughly determined by the bare Ti-SiO2-Si film, and then combined with the plasmon resonance effect of the double-Ti ring structure, the ultra-broadband absorption effect of the target band can be achieved. According to the electromagnetic field result map of this absorber, the double Ti ring is the main exciter for propagating surface plasmon resonance (PSPR) and local surface plasmon resonance, and the excited states of Ti rings with different radii require different wavelength electromagnetic waves to excite. The near-field coupling and inter-ring resonance coupling between the periodic structures excited by the double-ring design greatly broadens the absorption bandwidth and produces the expected absorption effect.

In the simulation process, we used the finite-difference time-domain (FDTD) module of Lumerical software for the solution. In the setting of boundary conditions, the x and y directions were set to periodic boundary conditions to simulate the overall structure of the absorber, which can save computer arithmetic power and a lot of time cost; the z direction was set to perfect matching layer (PML) conditions to eliminate interference to ensure that the simulation results are free from external interference. The highest level of 8 is used for the mesh to ensure the accuracy of the results. The optical parameters of the materials are taken from the palik data model that comes with the simulation software [34]. The dielectric constant of metal Ti has a large imaginary part in the ultra-long-wave infrared band, and the ultra-thin ring structure

Optical Materials EXPRESS

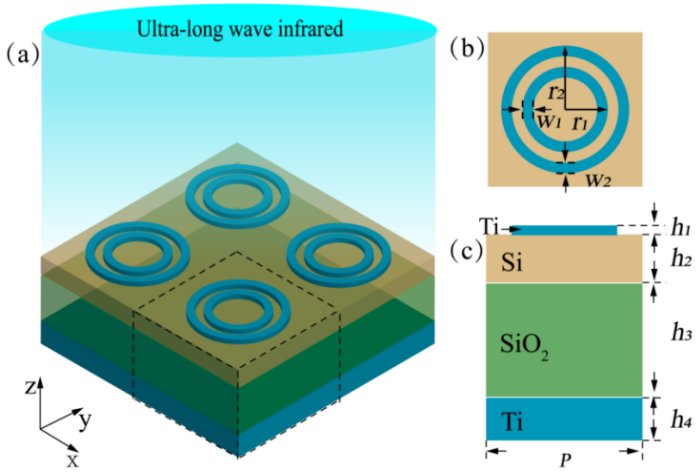

Fig. 1. (a) schematic diagram of the three-dimensional structure of MPA, (b) *x*-*y* planar structure, and circular radii $r_1 = 0.27$ μm, $r_2 = 0.36$ μm, with ring width $w_1 = w_2 = 55$ nm, (c) *x*-*z* planar structure with unit cell period $P = 0.9$ μm, per-layer thickness $h_1 = 20$ nm, $h_2 = 0.4$ μm, $h_3 = 1.28$ μm and $h_4 = 0.2$ μm

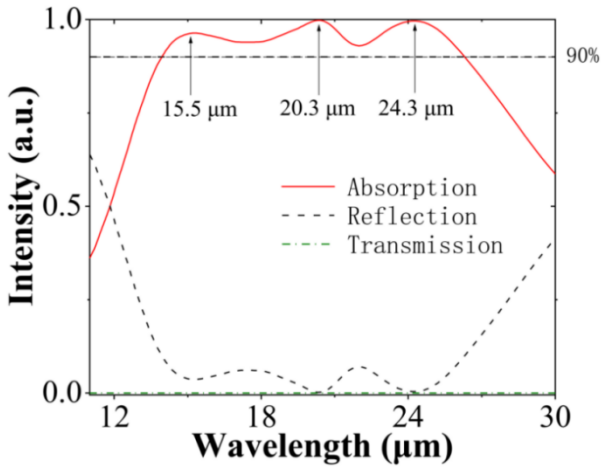

Fig. 2. Diagram of absorption (A), reflection (R) and transmission (T) intensities, with arrows representing the wavelengths at which the peaks are located

design provides an environment for the interaction between electromagnetic waves and matter; impedance matching is reached between various materials to finally achieve the ultra-broadband absorption effect. The structural parameters of the absorber are shown in Fig. 1 (b) and (c).

In the $A = 1\text{-}R\text{-}T$ absorption efficiency formula, A is the absorption rate, and R and T are the reflectance and transmittance, respectively. Since the metallic reflective layer essentially eliminates transmission, the absorption efficiency equation can be simplified to:

$$A = 1 - R \tag{1}$$

With reference to the above structural parameters, the absorption effect of the absorber in the excited state during the simulation is shown in Fig. 2. More than 90% absorption is achieved in the continuous band of 14.0-26.3 μm in the ULWIR, and the overall average absorption in this

Optical Materials EXPRESS

band is 96%, and the absorption in the last two wave peaks reaches more than 99.9%. According to the simulation results, the overall performance of the absorber is good in terms of absorption bandwidth and absorption effect.

3. Results and discussion

3.1. Bare Ti-SiO_2-Si film

Among the four-layer structure of the absorber MDDM, this section explores the structure of the bare Ti-SiO_2-Si film with its absorption curve, which is used to determine the approximate absorption range of the overall absorber, which is affected by the thickness of Si and SiO_2 in the composite media layer. The structure of the bare Ti-SiO_2-Si film and its absorption curve are shown in Fig. 3.

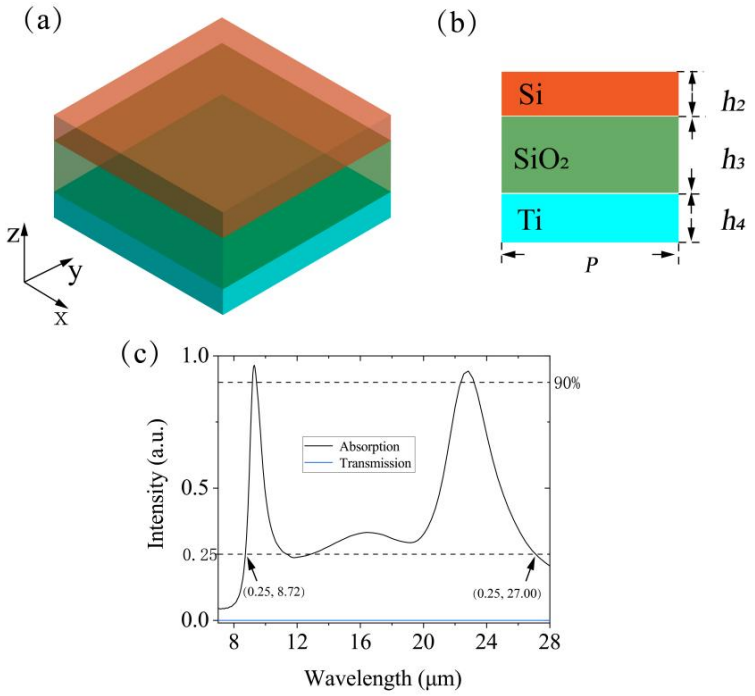

Fig. 3. (a) Schematic diagram of the structure of the bare Ti-SiO_2-Si film; (b) x-z planar structure with unit cell period $P = 0.9\,\mu m$, thickness of each layer $h_2 = 0.4\,\mu m$, $h_3 = 1.28\,\mu m$ and $h_4 = 0.2\,\mu m$; (c) absorption curves of the bare Ti-SiO_2-Si film

The absorption curve of the bare Ti-SiO_2-Si film has two absorption peaks, and from the two coordinates in Fig. 3(c), it can be seen that the band with absorption over 25% is 8.72-27.00 μm. On top of this, the approximate absorption range of the complete absorber after adding the top periodic structure is 8-30 μm, which lays the foundation for the absorption bandwidth of the absorber.

3.2. Number of resonant rings

In the absorber MDDM four-layer structure, due to the characteristics of the top periodic Ti ring and its inter-ring coupling resonance, there exists a large combination space for exploring the optimal combination of the number of rings that can be used in this absorber, and in this paper, simulations of single, double, triple and quadruple rings were done for the top Ti ring, and in

Optical Materials EXPRESS

order to maintain a stable coupling effect, the height of each ring was kept constant, and the radii of the four rings from outside to inside were 0.36 µm, 0.27 µm, 0.18 µm and 0.09 µm, and the width is referenced to the w value, and the absorption curves are compared graphically, and the results are shown in Fig. 4.

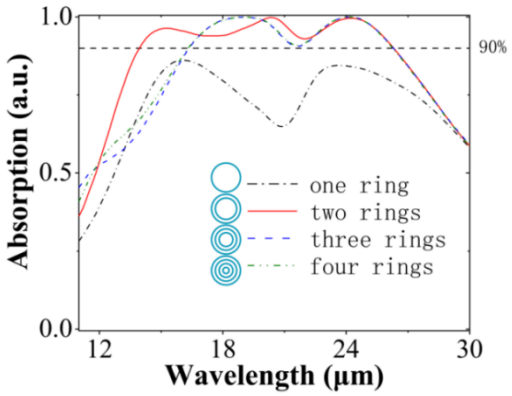

Fig. 4. Absorption intensity corresponds to a different number of resonant rings in the top layer

The individual curves in Fig. 4 show the absorption intensities and bandwidths corresponding to different ring numbers. The single ring has the worst absorption effect, with a better peak absorption effect of only 87% and a lower absorption intensity. The double resonant ring has the best absorption effect, with an average absorption intensity above 96% in the continuous absorption bandwidth of 14.0-26.3 µm. The curves of triple resonant ring and quadruple resonant ring basically overlap, and only in the absorption bandwidth of 16-26 µm the absorption intensity can reach more than 90%, and it is obviously weaker than the absorption effect of double ring resonance in the whole absorption band. From the analysis of the above results, the double-ring coupled resonant structure is the best choice for the top layer.

3.3. Physical mechanisms

The absorption principles of MPA are complex and diverse and can be analyzed in terms of the field distribution of electric and magnetic fields. The principles covered in this paper include SPR, inter-ring coupling resonance, near-field coupling between periodic structures, intrinsic absorption by lossy dielectric layers, and Fabry-Perot resonance cavity resonance. SPR means that when an infrared electromagnetic wave is incident on a periodic resonant ring structure, if the diffracted optical momentum at the surface of the resonant ring structure is equal to the propagation constant of the surface plasma, the diffracted light can be coupled with the surface plasma to achieve the broadband absorption effect of the absorber [36]:

$$\pm \mathrm{Re}(k_{sp}) = k_0(n_{d1} \sin\theta_1 + n_{d2} \sin\theta_2) + \frac{2\pi m}{P} \tag{2}$$

k_0 is the number of free space waves, n_{d1} is the refractive index of Si, n_{d2} is the refractive index of SiO_2, θ_1 is the angle of incidence of the electromagnetic wave on Si, θ_2 is the angle of incidence at the junction of two dielectric layers, m is the diffraction order, and P is the period of a cell. SPR can also be divided into PSPR and LSPR. PSPR is excited on a continuous metal film or grating, and the resulting PSPs present in the evanescent waves of the underlying metal

Optical Materials EXPRESS

and dielectric layers, which can be expressed as [34]:

$$k_{psp} = k_0(n_{d1}\sin\theta_1 + n_{d2}\sin\theta_2) + \frac{2\pi m}{P} - \frac{(n_{d1}h_2\cos\theta_1 + n_{d2}\cos\theta_2)}{m} \tag{3}$$

where h_1 is the thickness of Si and h_2 is the thickness of SiO_2. The LSPR is a localized surface plasmon resonance. It is excited at the surface of a periodic metallic Ti ring, and the LSPs is an evanescent wave around the Ti ring. LSPR can transfer the energy of photons to the surface plasma and greatly reduce reflections. Inter-ring coupled resonance is composed of two or more vibrating systems whose interaction can greatly improve the absorption effect and absorption bandwidth of the absorber. Periodic structural near-field coupling consists of interactions between periodic top particles and can be described as positive feedback of the periodic structure on the result. The intrinsic absorption of the lossy medium SiO_2 is due to its large imaginary part of the dielectric constant in the long wave infrared to ULWIR, which can absorb part of the electromagnetic waves and plays an important role in the resonant cavity and is the main region where the cavity resonance occurs. Finally, as a whole, the upper and lower metal layers and the insulating dielectric layer constitute the Fabry-Perot resonant cavity, which makes the absorption in the resonant state better.

Based on the results of the absorption intensity profile in Fig. 2, the physical mechanism of the absorber was further investigated using three absorption peaks in the absorption bandwidth of the absorber, and the cause of the absorption effect was analyzed using the excited electric and magnetic field maps on the peaks. The electric and magnetic field maps are taken from the *x*-*y* and *x*-*z* planes of a periodic cell of the absorber, as shown in Fig. 5, where (a)-(f) are electric field maps and (g)-(l) are magnetic field maps.

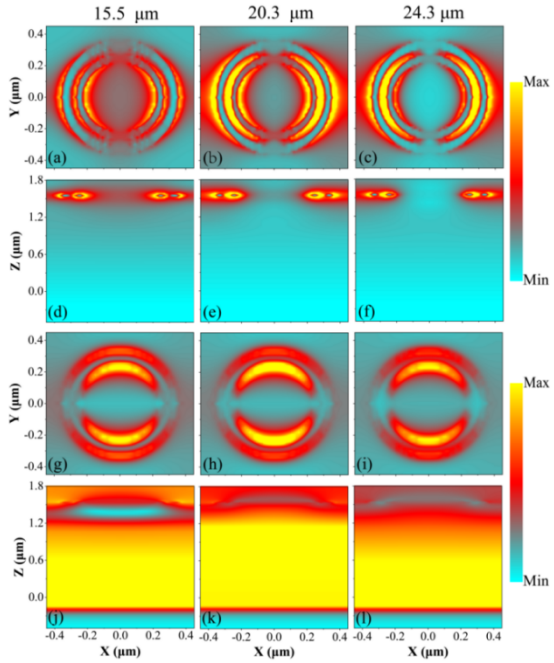

Fig. 5. (a-c) is the electric field distribution in the *x*-*y* plane, (d-f) is the electric field distribution in the *x*-*z* plane, (g-i) is the magnetic field distribution in the *x*-*y* plane, and (j-l) is the magnetic field distribution in the *x*-*z* plane; each column of images corresponds to 15.5 μm, 20.3 μm, and 24.3 μm wavelengths, respectively

Optical Materials EXPRESS

Compared with the absorption effect of the single resonant ring structure in Fig. 4, the absorber in the double resonant ring structure has a good absorption effect. From the three peak electromagnetic field plots in Fig. 5, it can be seen that the electric field intensity at the peak is clearly aggregated between the two rings, which indicates that the interaction of the coupled resonance between the rings can greatly enhance the absorption efficiency and absorption bandwidth of the absorber. To better illustrate the physical mechanism of the absorber, a detailed analysis of the EMF plots at each peak will be presented below.

At the first wave peak of 15.5 μm, the electric field intensity in Fig. 5(a) and (d) is mainly concentrated within the Ti inner ring, indicating that the absorption effect of this wave is dominated by the absorption of LSPR and inter-ring coupling resonance. The magnetic fields in Figs. 5(g) and (j) are mainly concentrated within the double resonant ring and the whole SiO_2 dielectric layer, indicating that the absorption effect of this wave also involves PSPR, Fabry- Perot resonance and the inherent absorption of SiO_2. Similarly, at the second peak at 20.3 μm, the electric field intensity in Fig. 5(b) and (e) shifts toward the outer ring, concentrating outside the outer ring, between the two rings and within the inner ring, indicating that the absorption effect at this peak is dominated by the LSPR, inter-ring coupling resonance and near-field coupling between the periodic structures. The absorption effect of this peak is also enhanced by the PSPR, the intrinsic absorption of SiO_2 and the synergistic resonance of the Fabry-Perot resonant cavity, as the magnetic field in Fig. 5(h) and (k) moves toward the inner ring in the x-y direction and toward the dielectric layer in the x-z direction and is mainly concentrated on both rings and the whole dielectric layer. In the third peak at 24.3 μm, the electric field intensity in Fig. 5(c) and (f) continues to move out of the ring, concentrating outside the outer ring and between the two rings, indicating that the absorption effect of this peak is dominated by the LSPR, inter-ring coupling resonance, and near-field coupling between the periodic structures. And the magnetic fields in Fig. 5(i) and (l) are concentrated in the dielectric layer, indicating that the absorption effect of this peak is also dominated by the PSPR, the intrinsic absorption of SiO_2, and the synergistic resonance of the Fabry-Perot resonant cavity, and the effect of the PSPR and resonant cavity is further enhanced. The analysis shows that as the infrared wavelength increases, the ring of response wavelength changes from the inner ring to the outer ring, indicating that the longer the wavelength, the larger the radius of the excited ring; the main role of the composite dielectric layer Si layer is to control the absorption dominated by surface plasmon resonance (SPR), SiO_2 has a certain intrinsic absorption and is the main location of the resonance effect in the main cavity layer; the underlying metal can play the role of complete reflection of electromagnetic waves to enhance the absorption effect of the absorber.

3.4. Optimization of structural parameters

The absorption effect of MPA is closely related to their structural parameters. The final parameters of the structure should ensure the best absorption effect. However, the initially designed structural parameters often do not achieve the best absorption effect, so we need to change the parameters of each layer in the MPA structure one by one and optimize them one by one to find the best absorption effect. The optimization is performed in the order from inner ring to outer ring and from top to bottom, which saves time in the optimization process. When performing the optimization, only one parameter of one of the structures is optimized in the first step, and the other parameters are set according to the initial parameters, after which the optimization is performed in the order of optimization and the optimized parameters from the previous step are applied to this optimization until the parameter optimization of the whole structure is completed. The optimization results are shown in Fig. 6.

In Fig. 6(a), the results of optimizing the ring width w_1 of the inner ring $Ring_1$ with other structural parameters unchanged are shown. The absorption effect of the absorber becomes progressively better as w_1 becomes progressively larger, and the absorption intensity of the

Optical Materials EXPRESS

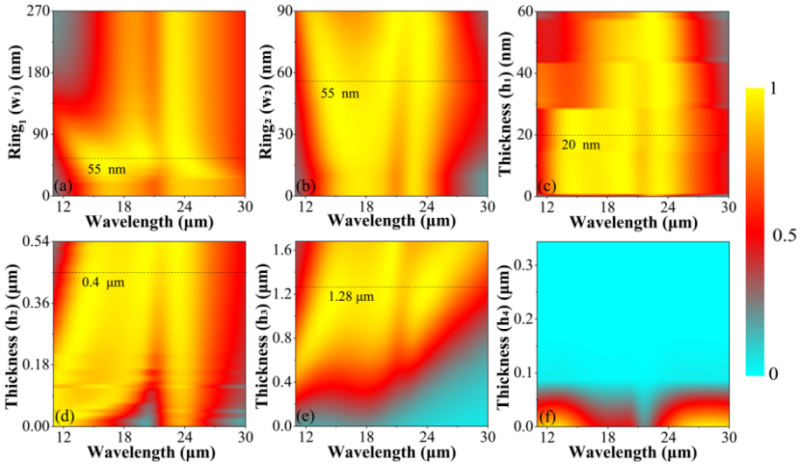

Fig. 6. Absorption intensity of MPA with optimization of each parameter. (a) is the parameter optimization of the $Ring_1$ width w_1, (b) is the parameter optimization of the $Ring_2$ width w_2, (c) is the parameter optimization of the ring height h_1, (d) is the parameter optimization of the Si thickness h_2, (e) is the parameter optimization of the SiO_2 thickness h_3, (f) is the thickness of the metal reflection layer h_4.

absorber is strongest when its ring width w_1 is 55 nm, while the absorption effect becomes progressively weaker when w_1 is larger than 55 nm. Similarly, by analogy, in Figure 6(b), the best value of w_2 at 55 nm can be obtained by introducing the optimized w_1 and optimizing the ring width w_2 of $Ring_2$. The optimal thickness h_1 for a ring height of 20 nm is given in Figure 6(c). the optimal thickness h_2 for Si of 0.4 μm is given in Figure 6(d). the optimal thickness h_3 for SiO_2 of 1.28 μm is given in Figure 6(e). Figure 6(f) shows the transmittance diagram of the absorber. Transmittance can be avoided as long as a certain thickness of the underlying metal Ti can be guaranteed, and here h_4 is taken as 0.2 μm.

3.5. *Influence of the incident light source state on absorption performance*

The practical application of MPA requires consideration of its performance under complex natural environmental conditions. Since various forms of polarization and infrared wave incidence angles exist in the natural environment, which have an impact on the absorption performance of MPA, this paper verifies the excellent absorption performance of electromagnetic waves at incidence angles of 0-60° and polarization angles of 0-90°, demonstrating the broad incidence angle and polarization independence of the absorber. The results are as follows.

In Fig. 7(a), the x-polarized light is incident at an inclination angle of 0-60°, and the absorption effect of the absorber is basically unchanged when the incident angle is less than 40°. When the incidence angle is greater than 40°, the absorption band starts to move to the left, and there is still a large absorption bandwidth and absorption effect at an incidence angle of 40°-60°. In Fig. 7(b), the y-polarized light is incident at an inclination angle of 0-60°, and the absorption effect of the absorber starts to weaken at an incidence angle of 40°, but still has a good absorption effect at an incidence angle of 40°-60°. Both show that this absorber can still absorb large wide-angle incident light with good effect at different polarization states. In the case of Fig. 7(c), the absorption bandwidth and absorption intensity are almost constant when the polarization angle is varied from 0-90°, showing excellent polarization independence. These three points provide the basis for the application of this absorber in complex natural environments.

Optical Materials EXPRESS

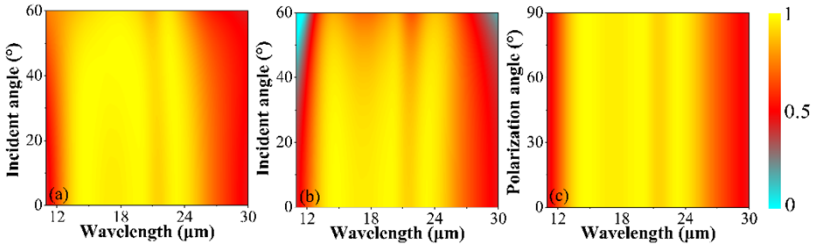

Fig. 7. (a) Variation of absorption intensity at 0-60° x-polarized light incidence, (b) variation of absorption intensity at 0-60° y-polarized light incidence, (c) variation of absorption intensity for incident light polarization angle of 0-90°

4. Conclusion

In this paper, a MPA based on multiple resonant rings with composite dielectric layers is designed and simulated, which can achieve more than 90% absorption in a continuous broadband of 12 μm in ULWIR (14.0-26.3 μm), with an average absorption rate above 96%, and the latter two peaks can achieve close to 99.9% absorption. In the paper, a control group was made for the number of pairs of resonant rings, and it was found that the double resonant ring absorber functioned best. The physical mechanism of absorption effect of the absorber is analyzed by electric field diagram and magnetic field diagram, and the resonance effect of each component and the overall structure are described, showing that the absorption curve is dominated by different resonance mechanisms and the overall resonance modes are complex and diverse, presenting a composite synergistic absorption mode. In order to cope with the complex natural environment, the wide-angle incidence range under different polarization modes and the influence of polarization angle on the absorber performance are analyzed, and the results show that the absorber has excellent wide-angle incidence absorption performance (0-60°) and is not affected by polarization. The effect of this absorber applied to the field of remote sensing can form a multi-level, multi-perspective, multi-domain observation system for global detection and monitoring from ground to air and even space, from information data collection and processing to interpretation, analysis and application, and become an important means to obtain information about the earth's resources and environment.

Funding. National Natural Science Foundation of China (61705127).

Disclosures. The authors declare that there are no conflicts of interest related to this article.

Data availability. Data underlying the results presented in this paper are available in Ref. [35].

References

1. Y. Li, Z. Li, Y. Liu, Y. Kong, and L. Huang, "Broadband and highly efficient polarization conversion in infrared region using plasmonic metasurfaces," Opt. Mater. **98**, 109420 (2019).
2. X. Cai, R. Tang, H. Zhou, Q. Li, S. Ma, D. Wang, T. Liu, X. Ling, W. Tan, Q. He, S. Xiao, and L. Zhou, "Dynamically controlling terahertz wavefronts with cascaded metasurfaces," Adv. Photonics **3**(03), 036003 (2021).
3. Z. Li, X. Cai, L. Huang, H. Xu, Y. Wei, and N. Dai, "Controllable Polarization Rotator with Broadband High Transmission Using All-Dielectric Metasurfaces," Adv. Theory Simul. **2**(9), 1900086 (2019).
4. B. Wang, Y. He, P. Lou, and W. Xing, "Design of a dual-band terahertz metamaterial absorber using two identical square patches for sensing application," Nanoscale Adv. **2**(2), 763–769 (2020).
5. M. R. Forouzeshfard, S. Ghafari, and Z. Vafapour, "Solute concentration sensing in two aqueous solution using an optical metamaterial sensor," J. Lumin. **230**, 117734 (2021).
6. T. Xue, W. Liang, Y. Li, Y. Sun, Y. Xiang, Y. Zhang, Z. Dai, Y. Duo, L. Wu, K. Qi, B. N. Shivananju, L. Zhang, X. Cui, H. Zhang, and Q. Bao, "Ultrasensitive detection of miRNA with an antimonene-based surface plasmon resonance sensor," Nat. Commun. **10**(1), 28 (2019).
7. L. Lei, S. Li, H. Huang, K. Tao, and P. Xu, "Ultra-broadband absorber from visible to near-infrared using plasmonic metamaterial," Opt. Express **26**(5), 5686–5693 (2018).

Optical Materials EXPRESS

8. Y. Liu, H. Liu, Y. Jin, and L. Zhu, "Ultra-broadband perfect absorber utilizing a multi-size rectangular structure in the UV-MIR range," Results Phys. **18**, 103336 (2020).
9. W. Chen, Y. Gao, Y. Li, Y. Yan, J. Y. Ou, W. Ma, and J. Zhu, "Broadband Solar Metamaterial Absorbers Empowered by Transformer-Based Deep Learning," Adv. Sci. 2206718 (2023).
10. T. Maier and H. Brückl, "Wavelength-Tunable Microbolometers with Metamaterial Absorbers," Opt. Lett. **34**(19), 3012–3014 (2009).
11. S. A. Kuznetsov, A. G. Paulish, A. V. Gelfand, P. A. Lazorskiy, and V. N. Fedorinin, "Bolometric THz-to-IR converter for terahertz imaging," Appl. Phys. Lett. **99**(2), 023501 (2011).
12. X. Liu, T. Starr, A. F. Starr, and W. J. Padilla, "Infrared spatial and frequency selective metamaterial with near-unity absorbance," Phys. Rev. Lett. **104**(20), 207403 (2010).
13. J. Hao, L. Zhou, and M. Qiu, "Nearly total absorption of light and heat generation by plasmonic metamaterials," Phys. Rev. B **83**(16), 165107 (2011).
14. Y. Cui, Y. He, Y. Jin, F. Ding, L. Yang, Y. Ye, S. Zhong, Y. Lin, and S. He, "Plasmonic and metamaterial structures as electromagnetic absorbers," Laser Photonics Rev. **8**(4), 495–520 (2014).
15. N. Mou, B. Tang, J. Li, Y. Zhang, H. Dong, and L. Zhang, "Demonstration of thermally tunable multi-band and ultra-broadband metamaterial absorbers maintaining high efficiency during tuning process," Materials **14**(19), 5708 (2021).
16. P. Zamzam, P. Rezaei, and S. A. Khatami, "Quad-band polarization-insensitive metamaterial perfect absorber based on bilayer graphene metasurface," Phys. E (Amsterdam, Neth.) **128**, 114621 (2021).
17. E. Hou, Z. Qin, Zh. Liang, D. Meng, X. Shi, F. Yang, W. Liu, H. Liu, H. Xu, D. R. Smith, and Y. Liu, "Dual-band metamaterial absorber with a low-coherence composite cross structure in mid-wave and long-wave infrared bands," Opt. Express **29**(22), 36145–36154 (2021).
18. I. Massiot, N. Vandamme, N. Bardou, C. Dupuis, A. Lemaître, J. F. Guillemoles, and S. Collin, "Metal nanogrid for broadband multiresonant light-harvesting in ultrathin GaAs layers," ACS Photonics **1**(9), 878–884 (2014).
19. J. Liu, W. Chen, W. Z. Ma, Y. S. Chen, X. C. Deng, P. P. Zhuang, and Q. Ye, "Biaxial hyperbolic metamaterial THz broadband absorber utilizing anisotropic two-dimensional materials," Results Phys. **22**, 103818 (2021).
20. N. Mou, X. Liu, T. Wei, H. Dong, Q. He, L. Zhou, Y. Zhang, L. Zhang, and S. Sun, "Large-scale, low-cost, broadband and tunable perfect optical absorber based on phase-change material," Nanoscale **12**(9), 5374–5379 (2020).
21. Y. Cheng, M. Xiong, M. Chen, S. Deng, H. Liu, C. Teng, H. Yang, H. Deng, and L. Yuan, "Numerical Study of Ultra-Broadband Metamaterial Perfect Absorber Based on Four-Corner Star Array," Nanomaterials **11**(9), 2172 (2021).
22. F. Chen, Y. Cheng, and H. Luo, "A broadband tunable terahertz metamaterial absorber based on single-layer complementary gammadion-shaped graphene," Materials **13**(4), 860 (2020).
23. T. Wang, H. Zhang, Y. Zhang, and M. Cao, "A bi-tunable switchable polarization-independent dual-band metamaterial terahertz absorber using VO2 and Dirac semimetal," Results Phys. **19**, 103484 (2020).
24. Z. Li, C. Luo, G. Yao, J. Yue, J. Ji, J. Yao, and F. Ling, "Design of a concise and dual-band tunable metamaterial absorber," Chin. Opt. Lett. **14**, 102303 (2016).
25. N. I. Landy, S. Sajuyigbe, J. J. Mock, D. R. Smith, and W. J. Padilla, "Perfect metamaterial absorber," Phys. Rev. Lett. **100**(20), 207402 (2008).
26. X. Liu, Z. Li, and Z. Wen, *et al.*, "Large-area, lithography-free, narrow-band and highly directional thermal emitter," Nanoscale **11**(42), 19742–19750 (2019).
27. Z. Yi, J. Li, J. Lin, F. Qin, X. Chen, W. Yao, Z. Liu, S. Cheng, P. Wue, and H. Lif, "Broadband polarization-insensitive and wide-angle solar energy absorber based on tungsten ring-disc array," Nanoscale **12**(45), 23077–23083 (2020).
28. S. Shrestha, Y. Wang, A. C. Overvig, M. Lu, A. Stein, L. D. Negro, and N. Yu, "Indium tin oxide broadband metasurface absorber," ACS Photonics **5**(9), 3526–3533 (2018).
29. C. H. Fann, J. Zhang, M. ElKabbash, W. R. Donaldson, E. M. Campbell, and C. Guo, "Broadband infrared plasmonic metamaterial absorber with multipronged absorption mechanisms," Opt. Express **27**(20), 27917–27926 (2019).
30. Y. Cui, K. H. Fung, J. Xu, H. Ma, Y. Jin, S. He, and N. X. Fang, "Ultrabroadband light absorption by a sawtooth anisotropic metamaterial slab," Nano Lett. **12**(3), 1443–1447 (2012).
31. S. Yue, M. Hou, R. Wang, H. Guo, Y. Hou, M. Li, Z. Zhang, Y. Wang, and Z. Zhang, "Ultra-broadband metamaterial absorber from ultraviolet to long-wave infrared based on CMOS-compatible materials," Opt. Express **28**(21), 31844–31861 (2020).
32. J. Liu, C. Dou, W. Chen, W. Z. Ma, D. Meng, X. Q. You, Y. S. Chen, P. H. Huang, and Y. Gu, "Inverse design a patternless solar energy absorber for maximizing absorption," Sol. Energy Mater. Sol. Cells **244**, 111822 (2022).
33. X. shi, E. Hou, Z. Liang, S. Zhang, R. Dai, W. Xin, D. Meng, H. Liu, H. Xu, and Y. Liu, "Broadband metamaterial absorber based on hybrid multi-mode resonance in mid-wave and long-wave infrared region," Results Phys. **42**, 105972 (2022).
34. Y. Zhou, Z. Qin, Z. Liang, D. Meng, H. Xu, D. R. Smith, and Y. Liu, "Ultra-broadband metamaterial absorbers from long to very long infrared regime," Light: Sci. Appl. **10**(1), 138 (2021).
35. E. D. Palik, *Handbook of Optical Constants of Solids* (Vol. 3) (Academic Press, 1998).
36. J. Homola, "Surface plasmon resonance sensors for detection of chemical and biological species," Chem. Rev. **108**(2), 462–493 (2008).